Science of the Total Environment 669 (2019) 505–511

Contents lists available at ScienceDirect

Science of the Total Environment

journal homepage: www.elsevier.com/locate/scitotenv

Plutonium fallout reconstructed from an Antarctic Plateau snowpack using inductively coupled plasma sector field mass spectrometry

Heejin Hwang [a], Soon Do Hur [a], Jeonghoon Lee [b], Yeongcheol Han [a,*], Sungmin Hong [c], Hideaki Motoyama [d,e]

[a] Korea Polar Research Institute, Incheon 21990, Republic of Korea
[b] Department of Science Education, Ewha Womans University, Seoul 03760, Republic of Korea
[c] Department of Ocean Sciences, Inha University, Incheon 22212, Republic of Korea
[d] National Institute of Polar Research, Tokyo 190-8518, Japan
[e] SOKENDAI (The Graduate University of Advanced Studies), Tokyo 190-8518, Japan

HIGHLIGHTS

- Atmospheric nuclear explosions in 1940–1980 caused global dispersion of plutonium.
- ICP-SFMS detected fallout ^{239}Pu from only a few grams of Antarctic Plateau snow.
- Purification and preconcentration of Pu were not necessary.
- Reconstructed ^{239}Pu fallout agreed with atmospheric nuclear explosion history.
- Potential of Pu as an atmospheric tracer and an age marker can be further utilized.

GRAPHICAL ABSTRACT

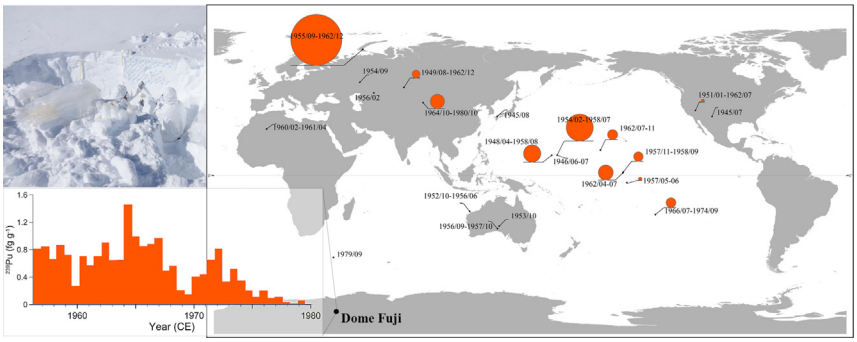

ARTICLE INFO

Article history:
Received 2 November 2018
Received in revised form 7 March 2019
Accepted 7 March 2019
Available online 9 March 2019

Editor: Mae Sexauer Gustin

Keywords:
Antarctic snow
Dome Fuji
Atmospheric nuclear test
Radionuclide
Ice core

ABSTRACT

Anthropogenic plutonium (Pu) in the environment is a result of atmospheric nuclear testing during the second half of the 20th century. In this work, we analyzed a 4-meter deep Antarctic Plateau snowpack characterized by a low snow accumulation rate and negligible snow impurities. These sample conditions enabled us to measure the snowpack Pu fallout by applying inductively coupled plasma sector field mass spectrometry to a few mL of snow melt without purification or preconcentration. Pu concentrations in the reconstructed Pu fallout record for the period after 1956 CE increased and decreased in agreement with past atmospheric nuclear testing. Two peaks and two dips associable with historical events were observed, and the highest peak in 1964(±1) CE approximately coincided with the maximum concentration of non-sea-salt sulfate caused by the Mt. Agung eruption in 1963 CE. Enhanced Pu fallout in the 1970s was attributed the geographical proximity of the Southern Hemispheric nuclear test sites. Our results suggest that by improving the instrumental sensitivity and precision, the potential of the Antarctic ice sheet as an archive of Pu fallout can be further explored and utilized for understanding atmospheric dispersion and for dating ice cores.

1. Introduction

Atmospheric nuclear explosions during the period from the 1940s to the 1980s are the major anthropogenic source of plutonium (Pu) in the

* Corresponding author.
E-mail address: yhan@kopri.re.kr (Y. Han).

https://doi.org/10.1016/j.scitotenv.2019.03.105
0048-9697/

environment. The radioactive Pu released from nuclear activities was spread globally via the atmosphere, and the Pu fallout can be detected in seawater, marine sediments (Koide et al., 1975; Lindahl et al., 2010), soil, river sediments (Tims et al., 2013), and ice cores from mid-latitude alpine glaciers (Gabrieli et al., 2011; Wang et al., 2017), the Arctic (Koide et al., 1985; Wendel et al., 2013), and Antarctica (Cutter et al., 1979; Koide et al., 1985). These natural archives preserve Pu fallout and evidence of changes in the flux during the period of atmospheric nuclear explosions.

The Antarctic Plateau represents a remote region isolated from the globally widespread atmospheric nuclear event sites (Fig. 1). Its overlying snowpack contains few impurities but has concentrated measurable levels of Pu fallout due to the low snow accumulation rate (<10 cm yr^{-1}). The Antarctic Plateau snowpack is therefore considered a prime historical archive in which to investigate the background level of Pu fallout and its temporal variation on a hemispheric to global scale (Cutter et al., 1979; Koide et al., 1979).

While pioneering research has been performed to reconstruct the historical records of Pu fallout using the Antarctic snowpack (Cutter et al., 1979; Koide et al., 1979), one great challenge has been measuring the extremely low levels of Pu (below a few fg g^{-1} (=10^{-15} g g^{-1}), 10^{-7} atoms g^{-1}, or μBq g^{-1}) in the snow. Previous studies used radioactivity counting methods (Cutter et al., 1979; Koide et al., 1979) or accelerated mass spectrometry (Koide et al., 1985), both of which required large sample amounts (10–100 kg), complicated pretreatments (e.g., Pu purification), and time-consuming instrumental analyses. Similar to using the maximum fallout of tritium (^3H) as an age indicator of 1966 (Jouzel et al., 1979; Kamiyama et al., 1989; Hoshina et al., 2014), those studies proposed the chronological potential of Pu for dating Antarctic snow (Koide et al., 1985). However, Pu has rarely been used chronologically because of the difficulty of measuring low levels of Pu.

In this study, we applied inductively coupled plasma sector field mass spectrometry (ICP-SFMS) to an Antarctic snowpack. Sensitivity improvements in ICP-SFMS have enabled the rapid detection of low Pu concentrations from a small amount of sample (Gabrieli et al., 2011). The purpose of this study was to examine the ability of ICP-SFMS to assess and utilize the potential of the Antarctic snowpack as a natural archive of ^{239}Pu fallout. Minimal sample pretreatment was performed on the Antarctic snow samples; thus, the Pu in the samples was not preconcentrated nor purified. Isobaric species that interfere with ^{239}Pu were carefully examined. Variations in the ^{239}Pu concentrations with snow depth were explored and compared with the nuclear test history and previous results from other Antarctic and Northern Hemispheric sites. Interhemispheric comparison is discussed in the context of the geographical distribution of the atmospheric nuclear tests. We also discuss the atmospheric implication and chronological application of the changes in the Pu fallout flux.

2. Material and methods

2.1. Sample description

A snow pit was dug at a site (77°18′ S, 39°47′ E, 3785 m a.s.l.) near Dome Fuji in Dronning Maud Land, East Antarctica, on December 10, 2007, during the Japanese-Swedish International Polar Year expedition. Successive snow samples were collected every 5 cm from the surface to a depth of 4 m (n = 80) by pushing a cylindrical polytetrafluoroethylene (PTFE) container into the vertical wall of the pit. The samples were poured into 500 mL low-density polyethylene (LDPE) bottles and double-sealed in LDPE bags. All the sampling tools were thoroughly precleaned in a clean laboratory at the Korea Polar Research Institute (KOPRI) following the protocol described by Hong et al. (2000) for trace element analysis. Multiple sets of successive samples were collected from same pit wall for various research purposes, including measurement of the water stable isotopes (Hoshina et al., 2014), physical properties (Fujita et al., 2012), aerosol particles (Iizuka et al., 2012) and trace elements. The trace element compositions of the samples used in this study were reported in several publications (Soyol-Erdene et al., 2011; Hong et al., 2012; Han et al., 2014; Chang et al., 2016). The previous studies all converted snow depth to age by identifying the pronounced non-sea-salt sulfate (nss-SO_4^{2-}) peaks produced by large volcanic eruptions, i.e., Mt. Pinatubo in June 1991 and Mt.

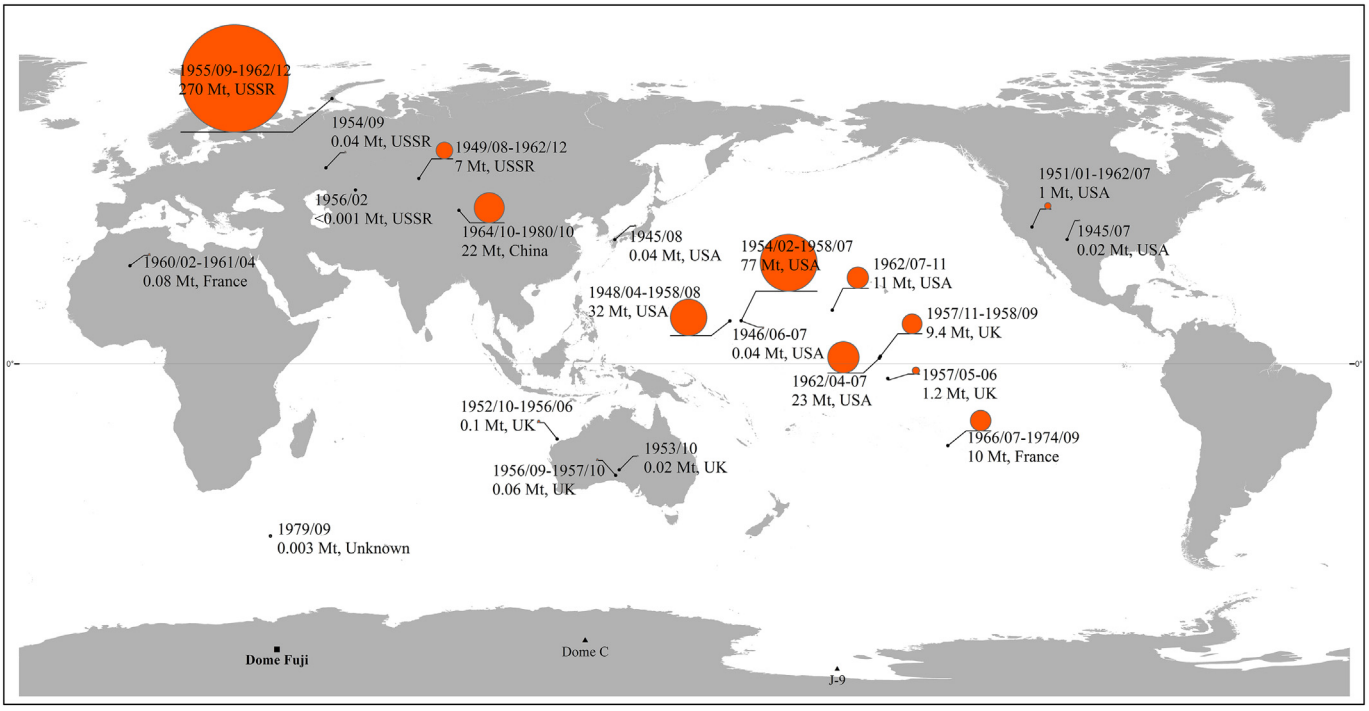

Fig. 1. Distribution of atmospheric nuclear activities during the period from the 1940s to the 1980s. The source data sets available in reference (Johnston, 2009) are grouped by site and date. Rocket- and missile-type tests with explosion heights >10 km were excluded. The size of the filled circles represents the sum of the estimated nuclear yield for each group. The sampling site (Dome Fuji, filled square) and previous study sites (J-9 and Dome C, filled triangles) are indicated.

Agung in March 1963 (Fig. 2b). We applied the depth-age relationship reported by Chang et al. (2016) to compare the Pu depth profile with the atmospheric nuclear test records.

2.2. Sample preparation

The frozen snow samples were transported to KOPRI. To avoid contamination, the samples were handled under clean conditions: class-10 clean benches in class-1000 clean laboratories at KOPRI (Hong et al., 2000). The samples were melted at room temperature, divided into 15 mL precleaned LDPE bottles, acidified to 1% (v/v) with ultrapure nitric acid (Optima grade, Fisher) and frozen until analysis.

2.3. Analytical procedure

To determine the Pu concentrations in the Antarctic Plateau snow samples, we used an ICP-SFMS (Element2, Thermo Scientific, Bremen, Germany) coupled with an Apex high-efficiency sample introduction system (Apex HF, ESI, USA). The instruments were installed in a HEPA-filtered clean booth inside a class-1000 clean laboratory. The system was tuned daily to achieve the maximum instrumental sensitivity (typically ~0.9×10^6 counts per second for a 100 pg mL^{-1} indium solution). The Pu concentration was measured in the low-resolution (LR, m/Δm ~ 300; Fig. S1) mode of the instrument to utilize its maximum sensitivity. The optimized instrument conditions for the determination of Pu are summarized in Table 1.

Uranium (U) was used as an external standard for the determination of the Pu concentration in a sample, which is applicable when standard Pu material is not available (Gabrieli et al., 2011). This method is based on the similar degrees of ionization (~99%) and first ionization energies of U and Pu (6.19 and 6.02 eV, respectively), meaning these elements behave similarly when ionized in the plasma (Lariviere et al., 2006). Several previous studies have shown similar instrumental sensitivities for U and Pu in ICP-MS systems (Baglan et al., 2000; Burraston, 2015) and have applied this approach to Pu quantification (Rondinella et al., 2000; Gabrieli et al., 2011; Arienzo et al., 2016; Winstrup et al., 2017). However, we note that our measurements are semiquantitative and focus more on the variations with depth rather than the absolute values.

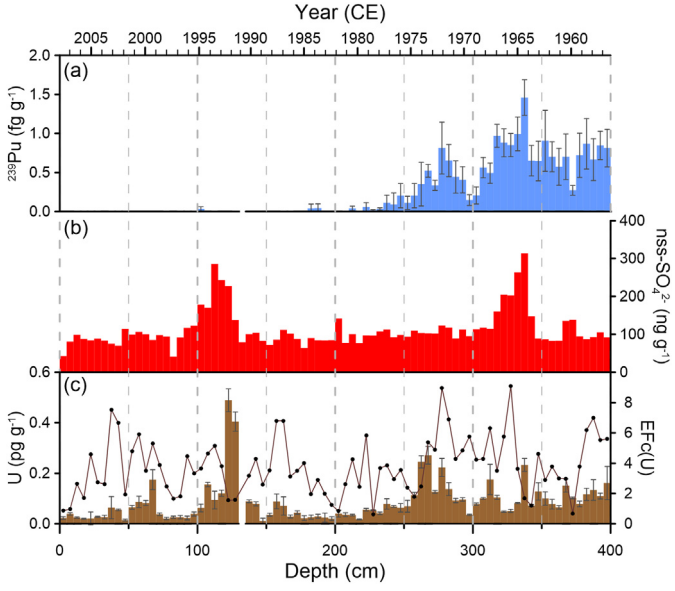

Fig. 2. Depth profiles of the (a) ^{239}Pu, (b) nss-SO_4^{2-}, and (c) U concentrations (bars), as well as the U enrichment factor (EFc(U), line). The x-axis is shown only for the depth intervals analyzed. The error bars indicate the 95% confidence intervals of the 12 *runs*. The snow depth-age relationship is shown at the top.

Table 1
Instrumentation and measurement parameters for the ICP-SFMS and desolvation system.

Element2-Apex HF	
Sampler/skimmer cones	Ni cones (H type)
Sample injector	Sapphire injector
Spray chamber	PFA cyclonic spray chamber
Nebulizer	PFA microflow (100 μL min^{-1}) nebulizer
Flow rates	
Cool gas (L min^{-1})	16
Auxiliary gas (L min^{-1})	0.7–0.8[a]
Sample gas (L min^{-1})	0.8–0.9[a]
Nitrogen (mL min^{-1})	~8[a]
Rinse out time (min)	6–10
Sample take-up time (s)	80
Target nuclides	^{208}Pb, ^{238}U, ^{239}Pu, ^{240}Pu, ^{238}U^{16}O
RF power (W)	1230
Resolution	Low (m/Δm ~ 300)
Scan type	Electric scans over small mass ranges (E-scan)
Runs and passes	12 × 3
Sample per peak	100
Mass/Integration window (%)	20/20
Integration type	Average
Dwell time per sample (ms)	10
Total acquisition time per peak (s)	0.2
Typical sensitivity	~0.9×10^6 cps for 100 pg g^{-1} indium solution

[a] Daily optimized.

Working standard solutions of U were prepared by sequentially diluting a 1000 μg g^{-1} stock solution (single element ICP standard, Inorganic Ventures, USA) to 0.1, 0.2, 0.5, 1, 2 and 10 pg g^{-1} in a 1% (v/v) HNO_3 matrix, and the solutions were used to calibrate both the U and Pu concentrations. The detection limits were calculated as three times the standard deviation of more than nine measurements of the 1% HNO_3. The detection limits were 0.005 pg g^{-1} and 0.053 fg g^{-1} for ^{238}U and ^{239}Pu, respectively. ^{238}U and ^{239}Pu counts for the 1% HNO_3 solution monitored during the sample measurement were equivalent to 0.004 pg g^{-1} and 0.008 fg g^{-1}, respectively. The calibration curve was verified using SLRS-5, a riverine water certified reference material (National Research Council of Canada, Ottawa, Canada). We determined the U concentrations in 500-fold (0.18 pg U g^{-1}) and 100-fold (0.94 pg U g^{-1}) diluted solutions and an undiluted solution of SLRS-5, and the recoveries were 109% (±5%, $n = 7$), 116% (±4%, $n = 2$) and 103% (±2%, $n = 2$), respectively, relative to the compiled literature value of 93 (±6) pg g^{-1} (Heimburger et al., 2013).

Impurities in the samples can cause isobaric compounds to form in the plasma, and these compounds can interfere with the Pu measurement. The most likely interference comes from the $^{238}U^1H$ compound, which cannot be separated from ^{239}Pu in the LR mode. To examine the influence of the isobaric interference, we analyzed multiple ^{238}U solutions in the concentration range of 0.1–100 pg g^{-1} and checked the ^{238}U hydride formation rate. The mean $^{238}U^1H/^{238}U$ ratio was 2.3 (± 0.1) × 10^{-5}. Since the U concentrations in the samples were all below 0.5 pg g^{-1} (Fig. 2c), the isobaric contribution of $^{238}U^1H$ was expected to be <0.01 fg g^{-1}. The highest U concentrations (0.5 pg g^{-1}) occurred at depths of 120–130 cm in association with a large volcanic nss-SO_4^{2-} input, and ^{239}Pu was not detected. As minor isobaric species interfering with ^{239}Pu, $^{207}Pb^{16}O^{16}O$ and $^{204}Pb^{35}Cl$ were further examined. Lead solutions in the concentration range of 10–1000 pg g^{-1} were analyzed to evaluate the $^{207}Pb^{16}O^{16}O$ formation rate of 1.2 (±0.2) × 10^{-5} (fg $^{207}Pb^{16}O^{16}O$)/(pg Pb). The Pb concentrations in our samples were all below 34 pg g^{-1} (Chang et al., 2016), and the isobaric contribution was estimated to be <0.001 fg g^{-1}. For $^{204}Pb^{35}Cl$, we measured four 100 pg Pb g^{-1} solutions with Cl concentrations of 50, 100, 500, and 1000 ng g^{-1}. The $^{204}Pb^{35}Cl$/Cl ratios were 2.9 × 10^{-5} (fg $^{204}Pb^{35}Cl$)/(ng Cl) for 50 to 500 ng Cl g^{-1} and 5.1 × 10^{-5} for 1000 ng Cl g^{-1}. The isobaric contribution of $^{204}Pb^{35}Cl$ to ^{239}Pu was estimate to be <0.015 fg g^{-1} below 500 ng Cl g^{-1}. We did not correct for isotopic interference in this study.

2.4. Records of atmospheric nuclear weapons tests

We used the compiled database of atmospheric nuclear explosions available in Johnston (2009). The database offers a historical list of nuclear events with information on the site coordinates, date, testing country, type, and estimated nuclear yield for each event. These data were categorized based on the site and date and are illustrated in Fig. 1, in which rocket- and missile-type tests were excluded since their explosion heights were too high (mostly >41 km) to cause significant variations in ground-level fallout.

3. Results

Plutonium was mostly detected in the lower half of the snow pit (Fig. 2a). The ^{239}Pu concentration gradually increased from a depth of 200 cm to 280 cm (0.8 ± 0.3 fg g^{-1}) and then leveled off. A dip (0.1 ± 0.1 fg g^{-1}) occurred at a depth of 295–305 cm and was followed by a further increase to the maximum value of 1.5 ± 0.2 fg g^{-1} at a depth of 335–340 cm. Below that depth, the concentration decreased sharply and remained at approximately 0.7 fg g^{-1}, excluding a sudden dip (0.3 ± 0.1 fg g^{-1}) at a depth of 370–375 cm. In the upper half of the snow pit, trace amounts of ^{239}Pu (0.06 to 0.07 fg g^{-1}) were detected in three layers (100–105, 180–185 and 185–190 cm).

U concentrations in the samples also varied with depth (Fig. 2c). Large volcanic eruptions noticeably elevated the U content in the snow layers at depths of 120–130 cm (Mt. Pinatubo) and 335–340 cm (Mt. Agung). To examine the natural U input, we evaluated the crustal enrichment factor (EFc) of U as follow: $EFc(U) = (U/Fe)_{sample} / (U/Fe)_{upper\ continental\ crust}$. The upper continental crust composition was adopted from a reference (Wedepohl, 1995). The calculated EFc (U) values were mostly >1 over the period covered by our samples that indicated U sources in addition to the terrestrial natural source. Mining activities in the Southern Hemisphere are known to be a major source of additional U, as they have noticeably increased anthropogenic U deposition in Antarctica since the 1980s (Potocki et al., 2016). In our results, however, the mean U concentrations (0.11 pg g^{-1}) and EFc (4.2) for the pre-1980 period were slightly higher ($p < 0.04$) than for the later period (0.07 pg g^{-1} and 3.4). The enhanced U deposition before 1980 may indicate that the atmospheric nuclear tests were a possible U source, and this relationship is supported by a significant correlation between Pu and EFc(U) ($r > 0.7$) during the Southern Hemispheric nuclear test periods of 1956–1962 and 1967–1981 (Fig. 3d). Further analysis of U isotopes (^{235}U/^{238}U or ^{236}U/^{238}U) should be able to confirm the atmospheric nuclear tests as a nonterrestrial U source (Eigl et al., 2016), although larger sample amounts would be required to detect ^{235}U or ^{236}U in Antarctic snow.

4. Discussion

4.1. Comparison with the atmospheric nuclear test history

The Pu concentration depth profile was compared to the atmospheric nuclear test history using the snow depth-age relationship. Since the Pu yield of each atmospheric nuclear test is mostly unknown and the atmospheric dispersion of nuclear products is poorly understood, we focused on the prominent increases and decreases in Pu fallout and compare them with the temporal changes in the total nuclear yields (Fig. 3). Plutonium-239 concentrations were constant within the error range between 1956 and 1958 (Fig. 3d), during which time >180 tests, including ~10 tests in Australia, were conducted by the UK, USA, and USSR (Figs. 1 and 3). The ^{239}Pu dip in 1959 can be linked to the nuclear test moratorium from 1958 to 1960. In 1960, France performed its first nuclear test in Algeria and that test was followed by >180 worldwide tests, mostly performed by the USA and USSR, until 1963. Two large thermonuclear weapons were tested in Novaya Zemlya (74°N) by the USSR in October 1961 and December 1962, and the resulting maximum ^{239}Pu fallout was observed in 1964. The delay was likely caused by the long-range transport of the nuclear fallout product. Most nuclear tests have been underground since the Partial Test Ban Treaty (PTBT) was signed by the UK, USA, and USSR in 1963. As a result, ^{239}Pu fallout has gradually decreased since 1964. However, the fallout level increased in the early 1970s, because France and China continued atmospheric testing until 1974 and 1980, respectively. The last known atmospheric nuclear test occurred in China in October 1980, consistent with the rare occurrence of Pu in the upper half of the snow pit. Underground tests continued until the late 1980s, but their contribution to atmospheric ^{239}Pu was minimal. The ^{239}Pu fallout in approximately 1983 (Fig. 2a) is also detected in the Northern Hemisphere (Gabrieli et al., 2011), but the cause is unclear. Although the relative contribution of the Chinese tests in Lop Nor to the global Pu fallout is expected to have been insignificant before 1970 (Wang et al., 2017), the last atmospheric test in 1980 cannot be ruled out if the reduced global Pu fallout, the travel time of the nuclear fallout products and the possible uncertainty in the snow depth-age relationship are considered. The fallout observed for 1994–1995 could not be connected to any known cause.

4.2. Comparison with previous results from Antarctic glaciers

In Fig. 3, the Dome Fuji results are compared with previous results from Dome C and J-9 sites (Fig. 1) in order to explore the spatial and temporal consistency in the Pu fallout in Antarctica. Those records display the increasing and decreasing trends of ^{239}Pu in accord with the atmospheric nuclear test history. Unlike our results, however, the highest ^{239}Pu peaks in the other depth profiles were observed in the earliest stages (Fig. 3e-f). Those peaks were previously attributed to the USA nuclear tests in the Pacific, including Ivy Mike in 1952 and Castle Bravo in 1954 (Koide et al., 1979, 1985). We expect that our snow pit did not reach the depth of the greatest ^{239}Pu fallout, which occurred prior to 1956.

Although the variation patterns in the ^{239}Pu concentration were broadly consistent, the ages of the peaks and dips dated by the respective depth-age models differed slightly between the results (Fig. S2). Before linking the age discrepancies with the spatiotemporal heterogeneity in the Pu fallout, the uncertainties in the depth-age models of both our and previous studies should be verified. We used linear interpolation, assuming constant snow accumulation between the volcanic SO_4^{2-}-age tie points that introduces uncertainty to the interpolated intervals. In the previous studies, age dating was mainly based on the ^{210}Pb chronology (Cutter et al., 1979; Koide et al., 1979). This method also assumed constant snow accumulation, but this assumption can produce larger uncertainties in regions with less snow accumulation. In addition, even if snowfall is assumed to be uniform, nonlinear snow accumulation may be expected due to snow redistribution by wind. For example, according to the annual bamboo stake measurements at Dome Fuji, the wind-driven redistribution caused a large spatial variation in snow accumulation, ranging from 46% to 123% over 36 sites within an area of 0.01 km^2, and 24 sites even had a negative annual snow accumulation at least once during the period from 1995 to 2006 (Kameda et al., 2008). These field observations revealed that the depth of an isochronous layer could have a mean standard deviation of 23 cm in a surface snowpack. The snow accumulation rate of the Dome C snowpack (3.7 cm y^{-1} in water equivalent (w.e.); Cutter et al., 1979) was similar to that of the Dome Fuji snowpack (2.7 cm w. e. y^{-1}), and comparable uncertainty is expected. Since the snow accumulation rate at J-9 was approximately three times higher (8.9 cm w. e. y^{-1}; Koide et al., 1979), a lower uncertainty (17 cm) is expected if the same level of undulations in the snow layers is assumed. If these considerable uncertainties are taken into account, the inconsistency in the timing of the peaks and dips cannot be ascribed to spatiotemporal heterogeneity in the Pu fallout and should be investigated further with more precisely dated samples.

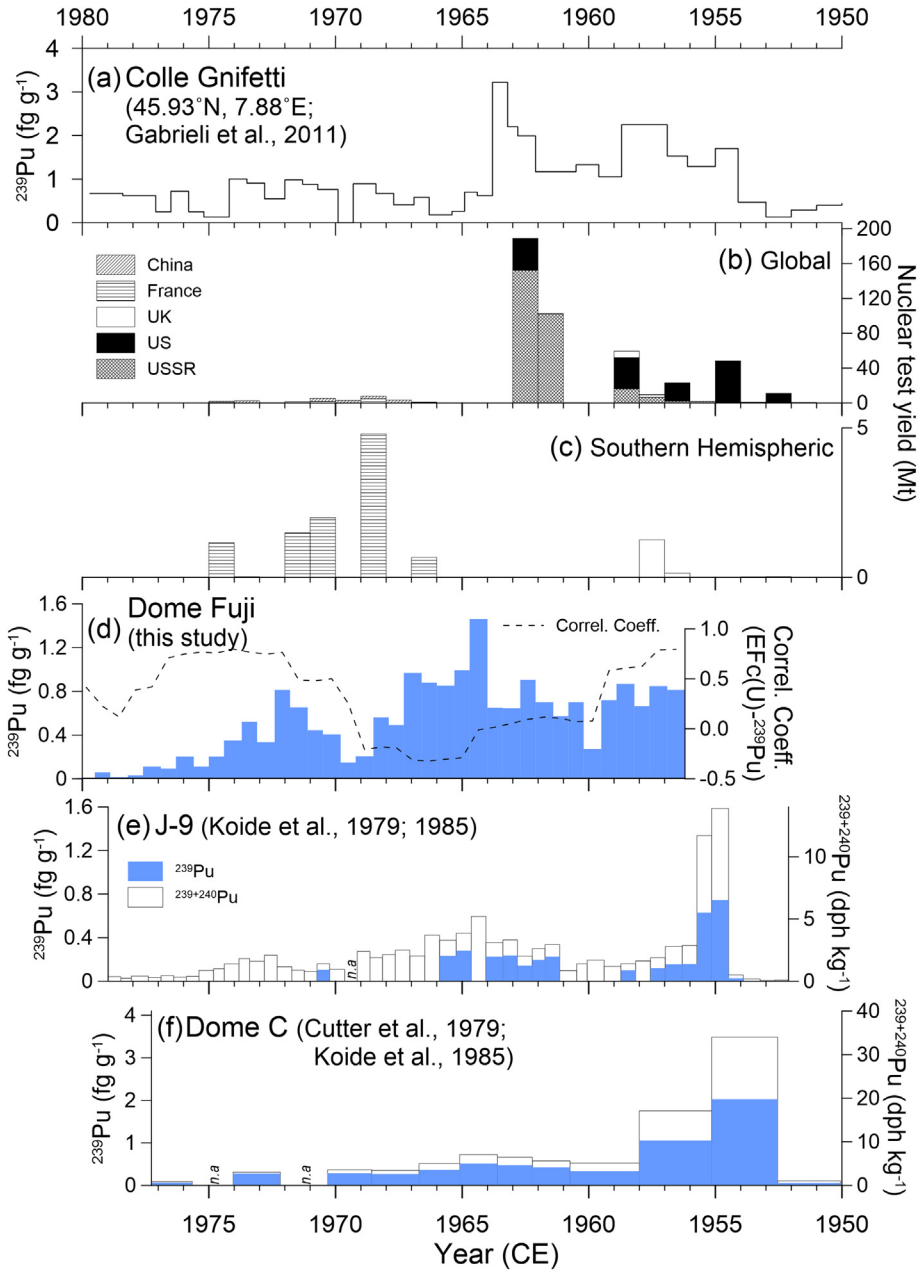

Fig. 3. (a, d–f) Reconstructed ^{239}Pu concentrations for the same periods at (a) Colle Gnifetti in the Alps and at (d) Dome Fuji, (e) J-9 and (f) Dome C, Antarctica. (b) Global and (c) Southern Hemispheric atmospheric nuclear yields by country and year from 1950 to 1980. For the Dome Fuji results, the 10-year moving correlation coefficient between EFc(U) and ^{239}Pu is shown (dashed line). The ^{239}Pu concentrations for J-9 and Dome C are calculated from the $^{239+240}$Pu activity (in disintegrations per hour (dph) kg^{-1}) (Koide et al., 1979; Cutter et al., 1979) and the ^{240}Pu/^{239}Pu ratios (Koide et al., 1985). For J-9, the ^{240}Pu/^{239}Pu ratio was reported for only 15 (of 48) samples in the reference (Koide et al., 1985). The depth-age models for J-9 and Dome C are refined relying on a nss-SO_4^{2-} peak dated to the year 1964 (see the text). *n.a.* indicates that the results for the depth intervals were not available in the references. The x-axes are displayed only for the periods covered by each study.

4.3. The distance dependence of the Pu fallout

The Pu temporal profile revealed that the distance from the nuclear test site is an important factor that affects the Pu concentration in the Antarctic Plateau snowpack. In the Southern Hemisphere, most of the nuclear tests were conducted from 1966 to 1975, and their total nuclear yields were less than one-tenth of the global yield in 1962 (Fig. 3c). However, the ^{239}Pu peaks produced by those tests (e.g., 0.86 fg g^{-1} in 1971–1972) were half as high as the largest peak (1.5 fg g^{-1} in 1964). Moreover, the EFc(U) values were generally elevated during the atmospheric nuclear test period (Fig. 2c), but their correlations with Pu were more pronounced between 1967 and 1981 ($r > 0.7$, $p < 0.001$) and between 1956 and 1962 ($r > 0.7$, $p < 0.015$) (Fig. 3d) when the relative contribution of the Southern Hemispheric tests is thought to have increased. These correlations suggest that the U was preferentially removed from the atmosphere during long-range transport from the Northern Hemisphere, unless only the Southern Hemispheric tests yielded proportional amounts of ^{238}U and ^{239}Pu.

The Pu fallout records preserved in Northern Hemisphere glaciers showed variations similar to those in the Antarctic glaciers; however, the geographical distribution of the nuclear test sites caused interhemispheric differences in the scale and timing of the Pu fallout. The intensive USSR nuclear tests in the Arctic (Novaya Zemlya, 74°N) from 1961 to 1962 led to the greatest ^{239}Pu fallout in Greenland and the

northern Alpine glaciers from 1963 to 1965 (Koide et al., 1985; Gabrieli et al., 2011; Fig. 3a). However, despite much higher nuclear yields (Fig. 3b), these tests produced a smaller peak in Antarctic glaciers than the US tests performed in the relatively close South Pacific (11°N) from 1952 to 1954 (Fig. 3e–f). The geographical differences meant that the travel time of the Pu released from the Arctic tests was longer than that released from the equatorial tests. This conclusion is supported by the fact that the ^{239}Pu peak in 1964, caused by the earlier 1961–1962 USSR tests, was concurrent with the nss-SO_4^{2-} peak from the later Mt. Agung (8°N) eruption in early 1963 (Fig. 2b) (Soyol-Erdene et al., 2011).

The distance dependence of the ^{239}Pu fallout is due to transport of the nuclear products via the troposphere rather than the stratosphere. The stratospheric residence time of Pu is 1.5 ± 0.5 years (Hirose and Povinec, 2015), and the distance dependence weakens once Pu is injected into the stratosphere. During a nuclear weapon test, the height to which the radioactive products can ascend depends on the nuclear test yield. It has been observed that when an explosion of tens to hundreds of kilotons occurs, the mushroom cloud can rise to below the tropopause. The nuclear products released from the relatively small Southern Hemispheric tests likely reached the study area in a shorter time via the troposphere than those transported via the stratosphere after originating from megaton-scale tests at remote sites. Consequently, the three-dimensional geographical distribution of the nuclear tests should be considered when interpreting fallout records.

4.4. Chronological implications and limitations

The chronological potential of Pu can be explored by comparing the Pu fallout record with age information derived from other indicators. The year 1964, with an error <±1 yr, was assigned to the largest ^{239}Pu peak, which was concurrent with the nss-SO_4^{2-} peak of the Mt. Agung eruption in 1963. This interpretation is consistent with the fact that the ^{3}H peak, corresponding to the year 1966 (Kamiyama et al., 1989; Pourchet et al., 2003; Hoshina et al., 2014), was identified 10–33 cm shallower than the Agung nss-SO_4^{2-} peak in the same snow pit (Hoshina et al., 2014). Due to the difference in phases between the gaseous HTO (tritiated water) and the particulate Pu, the broader ^{3}H fallout peak is expected to occur approximately 2 years later than the ^{239}Pu peak in the Antarctic Plateau (Jouzel et al., 1979; Koide et al., 1979). The earlier dip in ^{239}Pu was dated to 1960 (±1). This dip coincided with a small nss-SO_4^{2-} peak (365–375 cm, Fig. 2) previously attributed to the eruption of Cordón Caulle, Chile, in May 1960 (Hong et al., 2012). Based on their chronological compatibility with other age markers, we further suggest that the dip at 295–300 cm and the peak at 275–280 cm correspond to 1969 (±1) and 1971 (±1) detonations, respectively (Fig. 4), which are broadly consistent with the J-9 results (Fig. 3e). The uncertainty of ±1 year in the peak and dip timing was estimated based on the comparison with the J-9 results.

Since the nss-SO_4^{2-} peak in 1964 served as a solid age marker for the concurrent ^{239}Pu peak in the Dome Fuji results, the depth-age models of the J-9 and Dome C profiles could be further refined. Their adjusted ^{239}Pu profiles are shown in Fig. 3e–f. We added 2.1 years to the J-9 time scale to synchronize the 1964 ^{239}Pu peaks (Fig. 3e). For Dome C, the highest and second highest peaks were aligned with those in the adjusted J-9 profile (Fig. 3f). These alignments were within the uncertainty of the respective depth-age models described in Section 4.2. The refinement using the 1964 age tie point enhanced the correlation coefficient between the Dome Fuji ^{239}Pu record and the J-9 $^{239+240}$Pu record from 0.37 to 0.80 (Fig. S3).

Utilizing the Pu fallout record to date the Antarctic snowpack is expected to have two major advantages. First, introducing an independent age marker in addition to the volcanic nss-SO_4^{2-} peaks can reduce the uncertainty of the depth-age relationship and the possibility of misinterpreting temporal records of snow composition. This aspect is particularly significant on the Antarctic Plateau, where the snow accumulation rate is low (<~10 cm y^{-1}) and the undulations in isochronous snow layers are large due to wind-driven snow redistribution. Under these desert-like conditions, the seasonal cycles in the snowfall composition (e.g., δ^{18}O values and sea salt concentrations) (Hara et al., 2004; Fujita and Abe, 2006) are poorly preserved in the snowpack, and an annual layer counting method is often impractical (Soyol-Erdene et al., 2011; Hoshina et al., 2014). Additionally, Pu can be analyzed simultaneously with other elements of interest on an ICP-SFMS to provide age information about the target elements with minimal sample consumption. Other radionuclides may also have chronological potential, but separate analysis on larger samples is needed.

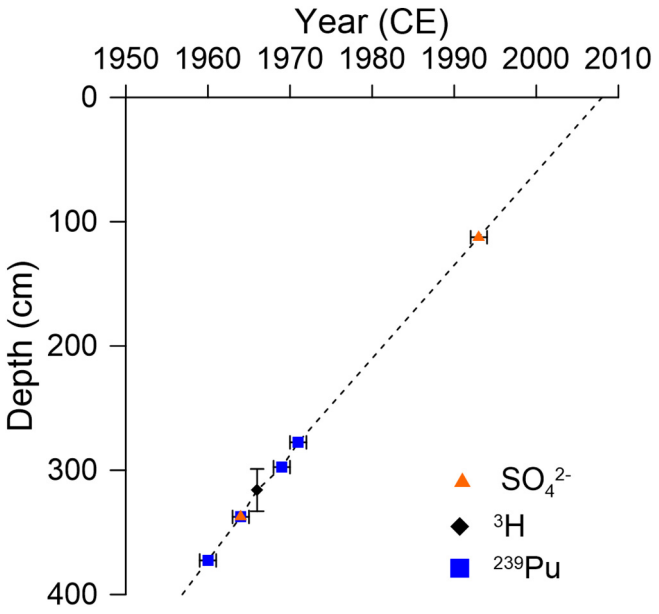

Fig. 4. Refined depth-age relationship based on the prominent ^{239}Pu peaks and dips.

From a practical perspective, the ages of the tie points (peaks and dips) should be further verified by precisely dating the fallout records. Generally, an ice core can be more accurately dated where the snow accumulation rate is high because the annual snow composition cycles are well preserved and easily counted. However, with a higher snow accumulation, the concentration of ^{239}Pu fallout in the snow will be lower, and detection of the peaks and dips will be difficult. Arienzo et al. (2016) used a continuous ice core melting method to introduce meltwater from an ice sample into an ICP-SFMS, and the detection limit for ^{239}Pu in this method was 0.24 fg g^{-1} (equivalent to 0.55 mBq kg^{-1}). They applied this method to six well-dated ice cores with accumulation rates ranging from 6.8 to 59.5 cm w.e. y^{-1}, but two peaks in the period from 1960 to 1980 were not detected due to the low ^{239}Pu content in the samples (Arienzo et al., 2016). In contrast, our results suggest that more precise analysis can reveal more ^{239}Pu peaks and dips with potential as age indicators. Our method, with the low detection limit of 0.053 fg g^{-1}, can be applied at a site with a snow accumulation rate higher than that at Dome Fuji. In future studies, further improvements in instrumental sensitivity, longer analysis times and/or preconcentration of the sample will be helpful for refining the precision and discerning the peaks and dips. Further research is needed on the spatial variation in the fallout flux to determine whether the ^{239}Pu peaks and dips occurred simultaneously and can be used as age indicators elsewhere in Antarctica. To demonstrate the full potential of Pu, however, a more precise measurement method needs to be applied to a well-dated ice core.

5. Conclusion

Coexisting isobaric species are the main concern in applying ICP-SFMS to quantification of ^{239}Pu in natural archives, and sample

pretreatment for Pu purification is generally required. Antarctic snowpack samples, however, contain negligible amounts of interfering species, and the low ^{239}Pu content is the single challenge that needs to be addressed. An ICP-SFMS instrument coupled with a desolvator was applied to measure the Pu in Antarctic Plateau snowpack samples that is relatively concentrated due to the low snow accumulation rate, and the detection of ^{239}Pu is achieved with only a few mL snow melt without purification or preconcentration. The reconstructed ^{239}Pu fallout record is associable with the atmospheric nuclear explosion history, with greater contributions from the more proximal Southern Hemispheric nuclear tests than the Northern Hemispheric tests. Moreover, the depth-age results broadly agree within uncertainty with previous reconstructions from other Antarctic sites, which supports the validity of using the ^{239}Pu peaks and dips as age markers for ice cores. Further application in higher snow accumulation areas, despite the lower ^{239}Pu concentrations in snow/ice, will lead to a more comprehensive understanding of the atmospheric transport of ^{239}Pu and the spatiotemporal homogeneity of its fallout in Antarctica.

Acknowledgments

We thank all the field personnel for sampling during the 48th and 49th Japanese Antarctic Research Expedition. This research was supported by a research grant (PE18040) from the Korea Polar Research Institute (KOPRI). The authors are grateful to the editor and reviewers for the valuable comments.

Appendix A. Supplementary data

Additional measurements of the ^{240}Pu/^{239}Pu ratio are described in the Supplementary material. Supplementary data associated with this article can be found in the online version, at doi: https://doi.org/10.1016/j.scitotenv.2019.03.105.

References

Arienzo, M.M., McConnell, J.R., Chellman, N., Criscitiello, A.S., Curran, M., Fritzsche, D., Kipfstuhl, S., Mulvaney, R., Nolan, M., Opel, T., Sigl, M., Steffensen, J.P., 2016. A method for continuous ^{239}Pu determinations in Arctic and Antarctic ice cores. Environ. Sci. Technol. 50, 7066–7073.

Baglan, N., Cossonnet, C., Pitet, P., Cavadore, D., Exmelin, L., Berard, P., 2000. On the use of ICP-MS for measuring plutonium in urine. J. Radioanal. Nucl. Chem. 243, 397–401.

Burraston, J.D., 2015. Advancing the analysis of low level uranium and plutonium in bioassay samples using SF-ICP-MS. Ph. D. Dissertation, University of Southampton, Southampton.

Chang, C., Han, C., Han, Y., Hur, S.D., Lee, S., Motoyama, H., Hou, S., Hong, S., 2016. Persistent Pb pollution in central East Antarctic snow: a retrospective assessment of sources and control policy implications. Environ. Sci. Technol. 50, 12138–12145.

Cutter, G.A., Bruland, K.W., Risebrough, R.W., 1979. Deposition and accumulation of plutonium isotopes in Antarctica. Nature. 279, 628–629.

Eigl, R., Steier, P., Winkler, S.R., Sakata, K., Sakaguchi, A., 2016. First study on ^{236}U in the Northeast Pacific Ocean using a new target preparation procedure for AMS measurements. J. Environ. Radioact. 162-163, 244–250.

Fujita, K., Abe, O., 2006. Stable isotopes in daily precipitation at Dome Fuji, East Antarctica. Geophys. Res. Lett. 33, L18503.

Fujita, S., Enomoto, H., Fukui, K., Iizuka, Y., Motoyama, H., Nakazawa, F., Sugiyama, S., Surdyk, S., 2012. Formation and metamorphism of stratified firn at sites located under spatial variations of accumulation rate and wind speed on the East Antarctic ice divide near Dome Fuji. The Cryosphere Discuss. 6, 1205–1267.

Gabrieli, J., Cozzi, G., Vallelonga, P., Schwikowski, M., Sigl, M., Eickenberg, J., Wacker, L., Boutron, C., Gäggeler, H., Cescon, P., Barbante, C., 2011. Contamination of Alpine snow and ice at Colle Gnifetti, Swiss/Italian Alps, from nuclear weapons tests. Atmos. Environ. 45, 587–593.

Han, Y., Huh, Y., Hong, S., Hur, S.D., Motoyama, H., 2014. Evidence of air-snow mercury exchange recorded in the snowpack at Dome Fuji. Antarctica. Geosci. J. 18, 105–113.

Hara, K., Osada, K., Kido, M., Hayashi, M., Matsunaga, K., Iwasaka, Y., Yamanouchi, T., Hashida, G., Fukatsu, T., 2004. Chemistry of sea-salt particles and inorganic halogen species in Antarctic regions: compositional differences between coastal and inland stations. J. Geophys. Res. 109, D20208.

Heimburger, A., Tharaud, M., Monna, F., Losno, R., Desboeufs, K., Nguyen, E.B., 2013. SLRS-5 elemental concentrations of thirty-three uncertified elements deduced from SLRS-5/SLRS-4 ratios. Geostandards Geoanal. Res. 37, 77–85.

Hirose, K., Povinec, P.P., 2015. Source of plutonium in the atmosphere and stratosphere-troposphere mixing. Sci. Rep. 5, 15707.

Hong, S., Lluberas, A., Rodriguez, F., 2000. A clean protocol for determining ultralow heavy metal concentrations: its application to the analysis of Pb, Cd, Cu, Zn and Mn in Antarctic snow. Korean J. Polar Res. 11, 35–47.

Hong, S., Soyol-Erdene, T.-O., Hwang, H., Hong, S.B., Hur, S.D., Motoyama, H., 2012. Evidence of global-scale As, Mo, Sb, and Tl atmospheric pollution in the Antarctic snow. Environ. Sci. Technol. 46, 11550–11557.

Hoshina, Y., Fujita, K., Nakazawa, F., Iizuka, Y., Miyake, T., Hirabayashi, M., Kuramoto, T., Fujita, S., Motoyama, H., 2014. Effect of accumulation rate on water stable isotopes of near-surface snow in inland Antarctica. J. Geophy. Res. Atmos. 119, 274–283.

Iizuka, Y., Tsuchimoto, A., Hoshina, Y., Sakurai, T., Hansson, M., Karlin, T., Fujita, K., Nakazawa, F., Motoyama, H., Fujita, S., 2012. The rates of sea salt sulfatization in the atmosphere and surface snow of inland Antarctica. J. Geophys. Res. Atmos. 117, D04308.

Johnston, W.R., 2009. Nuclear Tests – Databases and other material. http://www.johnstonsarchive.net/nuclear/tests/ (last modified 2 July 2009; accessed 29 October 2018).

Jouzel, J., Merlivat, L., Pourchet, M., Lorius, C., 1979. A continuous record of artificial tritium fallout at the South Pole (1954–1978). Earth Planet. Sci. Lett. 45, 188–200.

Kameda, T., Motoyama, H., Fujita, S., Takahashi, S., 2008. Temporal and spatial variability of surface mass balance at Dome Fuji, East Antarctica, by the stake method from 1995 to 2006. J. Glaciol. 54, 107–116.

Kamiyama, K., Ageta, Y., Fujii, Y., 1989. Atmospheric and depositional environments traced from unique chemical compositions of the snow over an inland high plateau, Antarctica. J. Geophy. Res. 94, 18515–18519.

Koide, M., Griffin, J.J., Goldberg, E.D., 1975. Records of plutonium fallout in marine and terrestrial samples. J. Geophy. Res. 80, 4153–4162.

Koide, M., Michel, R., Goldberg, E.D., 1979. Depositional history of artificial radionuclides in the Ross Ice Shelf. Antarctica. Earth Planet. Sci. Lett. 44, 204–223.

Koide, M., Bertine, K.K., Chow, T.J., Goldberg, E.D., 1985. The ^{240}Pu/^{239}Pu ratio, a potential geochronometer. Earth Planet. Sci. Lett. 72, 1–8.

Lariviere, D., Taylor, V.F., Evans, R.D., Cornett, R.J., 2006. Radionuclide determination in environmental samples by inductively coupled plasma mass spectrometry. Spectrochim. Acta Part B At. Spectrosc. 61, 877–904.

Lindahl, P., Lee, S.H., Worsfold, P., Keith-Roach, M., 2010. Plutonium isotopes as tracers for ocean processes: a review. Marine Environ. Res. 69, 73–84.

Potocki, M., Mayewski, P.A., Kurbatov, A.V., Simõoes, J.C., Dixon, D.A., Goodwin, I., Carleton, A.M., Handley, M.J., Jaña, R., Korotkikh, E.V., 2016. Recent increase in Antarctic Peninsula ice core uranium concentrations. Atmos. Environ. 140, 381–385.

Pourchet, M., Magand, O., Frezzotti, M., Ekaykin, A., Winther, J.-G., 2003. Radionuclides deposition over Antarctica. J. Environ. Radioactivity 68, 137–158.

Rondinella, V.V., Betti, M., Bocci, F., Hiernaut, T., Cobos, J., 2000. IC-ICP-MS applied to the separation and determination of traces of plutonium and uranium in aqueous leachates and acid rinse solutions of UO_2 doped with ^{238}Pu. Microchem. J. 67, 310–324.

Soyol-Erdene, T.-O., Huh, Y., Hong, S., Hwang, H., Hur, S.D., 2011. A 50-year record of platinum, iridium, and rhodium in Antarctic snow: volcanic and anthropogenic sources. Environ. Sci. Technol. 45, 5929–5935.

Tims, S.G., Fifield, L.K., Hancock, G.J., Lal, R.R., Hoo, W.T., 2013. Plutonium isotope measurements from across continental Australia. Nucl. Instrum. Method Phys. Res. B. 294, 636–641.

Wang, C., Hou, S., Pang, H., Liu, Y., Gäggeler, H.W., Christl, M., Synal, H.-A., 2017. ^{239,240}Pu and ^{236}U records of an ice core from the eastern Tien Shan (Central Asia). J. Glaciol. 63 (241), 929–935.

Wedepohl, K.H., 1995. The composition of the continental crust. Geochim. Cosmochim. Acta 59, 1217–1232.

Wendel, C.C., Oughton, D.H., Lind, O.C., Skipperud, L., Fifield, L.K., Isaksson, E., Tims, S.G., Salbu, B., 2013. Chronology of Pu isotopes and ^{236}U in an Arctic ice core. Sci. Total Environ. 461-462, 734–741.

Winstrup, M., Vallelonga, P., Kjær, H.A., Fudge, T.J., Lee, J.E., Riis, M.H., Edwards, R., Bertler, N.A.N., Blunier, T., Brook, E.J., Buizert, C., Ciobanu, G., Conway, H., Dahl-Jensen, D., Ellis, A., Emanuelsson, B.D., Keller, E.D., Kurbatov, A., Mayewski, P., Neff, P.D., Pyne, R., Simonsen, M.F., Svensson, A., Tuohy, A., Waddington, E., Wheatley, S., 2017. A 2700-year annual timescale and accumulation history for an ice core from Roosevelt Island. West Antarctica. https://doi.org/10.5194/cp-2017-101 (accepted).